HHS Public Access

Author manuscript

Brain Behav Immun. Author manuscript; available in PMC 2024 July 05.

Published in final edited form as:

Brain Behav Immun. 2024 July ; 119: 713–723. doi:10.1016/j.bbi.2024.04.015.

Neuroinflammation in post-acute sequelae of COVID-19 (PASC) as assessed by [^{11}C]PBR28 PET correlates with vascular disease measures

Michael B. VanElzakker[a,e,*], **Hannah F. Bues**[a], **Ludovica Brusaferri**[b,c], **Minhae Kim**[b], **Deena Saadi**[a], **Eva-Maria Ratai**[b], **Darin D. Dougherty**[a], **Marco L. Loggia**[b,d]

[a]Division of Neurotherapeutics, Department of Psychiatry, Athinoula A. Martinos Center for Biomedical Imaging, Massachusetts General Hospital, Harvard Medical School, Boston, MA, USA

[b]Department of Radiology, Athinoula A. Martinos Center for Biomedical Imaging, Massachusetts General Hospital, Harvard Medical School, Boston, MA, USA

[c]Department of Computer Science And Informatics, School of Engineering, London South Bank University, London, UK

[d]Department of Anesthesia, Critical Care and Pain Medicine, Massachusetts General Hospital, Harvard Medical School, Boston, MA, USA

[e]PolyBio Research Foundation, Medford, MA, USA

Abstract

The COVID-19 pandemic caused by SARS-CoV-2 has triggered a consequential public health crisis of post-acute sequelae of COVID-19 (PASC), sometimes referred to as long COVID. The mechanisms of the heterogeneous persistent symptoms and signs that comprise PASC are under investigation, and several studies have pointed to the central nervous and vascular systems as being potential sites of dysfunction. In the current study, we recruited individuals with PASC with diverse symptoms, and examined the relationship between neuroinflammation and circulating markers of vascular dysfunction. We used [^{11}C]PBR28 PET neuroimaging, a marker of neuroinflammation, to compare 12 PASC individuals versus 43 normative healthy controls. We found significantly increased neuroinflammation in PASC versus controls across a wide swath of brain regions including midcingulate and anterior cingulate cortex, corpus callosum, thalamus,

[*]Corresponding author at: 149 Thirteenth Street, Office 2610, Building 149, Martinos Center for Biomedical Imaging, Charlestown MA 02129, USA. mvanelzakker@mgh.harvard.edu (M.B. VanElzakker).

CRediT authorship contribution statement

Michael B. VanElzakker: Conceptualization, Funding acquisition, Writing – original draft, Writing – review & editing, Supervision. **Hannah F. Bues:** Formal analysis, Visualization, Writing – review & editing. **Ludovica Brusaferri:** Formal analysis, Writing – review & editing. **Minhae Kim:** Data curation, Writing – review & editing. **Deena Saadi:** Formal analysis, Writing – review & editing. **Eva-Maria Ratai:** Funding acquisition, Writing – review & editing. **Darin D. Dougherty:** Supervision. **Marco L. Loggia:** Formal analysis, Funding acquisition, Supervision, Writing – review & editing.

Declaration of Competing Interest

The authors declare that they have no known competing financial interests or personal relationships that could have appeared to influence the work reported in this paper.

Appendix A. Supplementary data

Supplementary data to this article can be found online at https://doi.org/10.1016/j.bbi.2024.04.015.

basal ganglia, and at the boundaries of ventricles. We also collected and analyzed peripheral blood plasma from the PASC individuals and found significant positive correlations between neuroinflammation and several circulating analytes related to vascular dysfunction. These results suggest that an interaction between neuroinflammation and vascular health may contribute to common symptoms of PASC.

Keywords

COVID-19; Long COVID pathogenesis; Neuroimaging; Positron emission tomography; Fibrinogen; Cardiovascular; Glia; Microglia; Brain inflammation

1. Introduction

The coronavirus disease 2019 (COVID-19) global pandemic caused by severe acute respiratory syndrome coronavirus 2 (SARS-CoV-2) has triggered a consequential public health crisis of long COVID or post-acute sequelae of COVID-19 (PASC), defined by symptoms that begin following acute SARS-CoV-2 infection or persist from that initial acute illness (Centers for Disease Control and Prevention, 2022; World Health Organization, 2021).

The US Census Bureau's Household Pulse Survey found that, as of June 2023, about 11% of adults who had ever had COVID-19 reported that they were currently experiencing symptoms of PASC or long COVID, with nearly 16% of adults stating that they had PASC or long COVID symptoms at some point in time (National Center for Health Statistics, 2023). PASC is an umbrella term applied to a heterogeneous group of patients. Symptoms can be diverse and commonly include nonspecific neurological and neuropsychiatric symptoms including difficulty concentrating or subjective 'brain fog,' unusually profound fatigue, headaches, depression, anxiety, body pain, and disrupted sleep (Davis et al., 2021; Zeng et al., 2023). These symptoms can significantly impact quality of life (Líška et al., 2022), and can be initiated even by mild acute COVID-19 illness (Boribong et al., 2022; Ma et al., 2023).

With evidence accumulating for coagulation and vascular-related problems in PASC (Klein et al., 2022; Pretorius et al., 2022; Proal & VanElzakker, 2021), it is a priority to understand how vascular and central nervous system problems may drive nonspecific neurological and neuropsychiatric symptoms in some PASC patients. As a densely vascularized organ that uses 15–20% of the body's total circulating blood supply (Berkman et al., 2021), the brain is uniquely vulnerable to disruptions to vascular health. COVID-19 appears to confer a potent vulnerability to neurovascular problems. For example, in patients that survived acute COVID-19, in the following year the risk for hemorrhagic stroke and for cerebral venous thrombosis more than doubled (Xie et al., 2022; Xu et al., 2022). As evidence of general consequences for the brain in PASC, a longitudinal study comparing pre-pandemic structural neuroimaging data to post-COVID structural neuroimages from the same individual showed small but significant reduction of grey matter thickness and whole-brain volume as well as increased markers of tissue damage, relative to longitudinal scans from individuals not infected with SARS-CoV-2 (Douaud et al., 2022). In PASC, a neuroimaging study using

arterial spin labeling fMRI found evidence of decreased neurovascular perfusion in patients reporting persistent cognitive problems (Ajčević et al., 2023). These observations could potentially relate to neuroinflammatory processes or vascular dysfunction, but no study has yet directly studied these two factors together.

In addition to their role as the innate immune cells of the central nervous system, glial cells are critical to normal central nervous system functioning, including playing a central role in neurotransmission, neurovascular function, and blood–brain barrier integrity. Thus, the activity of glial cells may be an important connection between brain and vascular abnormalities in PASC (Cabezas et al., 2014; Mestre et al., 2017). Like other innate immune cells, glia can enter a spectrum of 'activated' states when they detect paracrine inflammatory mediators (e. g., proinflammatory cytokines), pathogen-associated molecular patterns (PAMPs), or damage-associated molecular patterns (DAMPs). Short-term glial activation is central to their role as cells of innate, or nonspecific, immunity that clear multiple forms of pathogens or cell debris. The glial role in the innate immune system also involves general 'sickness' symptoms that shift an organism's behavior to preserve energy at a time of high energy demand (Dantzer & Kelley, 2007; VanElzakker et al., 2019). However, long-term glial activation can disrupt the delicate symbiosis of glia, blood vessels, neurons, and cerebrospinal fluid in normal central nervous system function, and ongoing glial activation occurs in multiple neurological and neuropsychiatric conditions (VanElzakker et al., 2019) and is associated with symptoms that are commonly reported in PASC such as disrupted cognition (Barrientos et al., 2006; Lindgren et al., 2020), increased pain (Loggia et al., 2015), and other nonspecific symptoms of sickness.

Activation of glia is a key component of neuroinflammation, which can include other mechanisms such as activated peripheral immune cells penetrating into brain, inflammatory activation of neurovascular endothelial cells, or density of motile microglia. Rodent models have shown upregulation of the translocator protein (TSPO) during glial activation states (Pannell et al., 2020), and PET neuroimaging with TSPO-specific radioligands is a widely used method in the study of human neuroinflammation (Albrecht et al., 2016; VanElzakker et al., 2019). [^{11}C]PBR28 is a second-generation TSPO-binding radioligand that has good specificity for TSPO and a low background signal-to-noise ratio (Albrecht et al., 2016).

2. Materials and methods

2.1. Study design

In this case-control, cross-sectional study, we compared 12 PASC versus an existing dataset of 43 control individuals with no known prior COVID-19 exposure. We used PET neuroimaging to study neuroinflammation (here operationalized as increased TSPO radioligand binding) in PASC by comparing [^{11}C]PBR28 standardized uptake value ratios (SUVR) in PASC versus controls. All participants answered questionnaires related to pain and depression; PASC participants answered additional questionnaires related to their PASC symptoms and history.

We also analyzed peripheral blood collected from PASC participants immediately before their PET scan to study the relationship between central nervous system glial activation

in PASC and measures related to vascular health, inflammation, and angiogenesis. For the blood measurements, platelet-poor plasma (PPP) was collected from 11 PASC cases immediately before [^{11}C]PBR28 injection.

2.2. Participants

As PASC is an umbrella term with a heterogeneous presentation, cohort phenotyping is key to study design. To prioritize recruitment of individuals with diverse nonspecific symptoms, we used a modified myalgic encephalomyelitis/chronic fatigue syndrome (ME/CFS) International Consensus Criteria (ICC, Carruthers et al., 2011) as PASC group inclusion criteria, requiring at least one symptom from each of the 4 ICC symptom clusters: post-exertion exhaustion, neurological impairments, immune/gastro-intestinal/genito-urinary, and energy/autonomic. All PASC participants had onsetting COVID-19 illness that occurred before August 2021 and at least 10 months prior to the scan date (mean = 20.50 months, *SD* = 7.75), reflecting pre-Omicron strains and qualifying them for both CDC and WHO definitions of PASC (4 weeks or 3 months of symptoms, respectively). Two of the 12 PASC participants were hospitalized during their acute COVID-19 (without being put on a ventilator), and 1 of 12 reported being vaccinated prior to the acute COVID-19 infection that initiated their PASC. No PASC or control participants were currently acutely ill.

A total of 12 PASC study participants were compared to an existing normative dataset of 43 healthy controls with no known history of COVID-19, that were scanned with the same protocol in the same scanner, between 2013–2021. During that time there were no software upgrades to the scanner and the only hardware changes made had been a minor modification for airflow, and an occasional detector replacement. The acquisition and processing protocols across all scans included in this analysis have been consistent, including image reconstruction parameters and attenuation correction method. Control scans were selected from multiple completed or ongoing studies (e.g., Albrecht et al., 2019; Alshelh et al., 2020; Loggia et al., 2015); 34 of the 43 controls were scanned pre-pandemic and all post-pandemic-onset controls had a negative plasma antibody test but were scanned in Massachusetts' state-of-emergency period of the pandemic (Brusaferri et al., 2022). Participants of any sex were recruited to participate in a ~90 min scanning session at the HST/MGH (Harvard-Massachusetts Institute of Technology Program in Health Sciences and Technology/Massachusetts General Hospital) A.A. Martinos Center for Biomedical Imaging, in Boston MA.

Exclusionary criteria included PET or MRI contraindications (e.g., metallic implants, surpassed FDA research-related PET scan limit in past 12 months, major kidney or liver problems, pregnancy), history of other neurological disorders (epilepsy, history of stroke, tumor, brain tissue-damaging pathologies), history of major head trauma (loss of consciousness for more than 5 min), type 1 diabetes, major cardiac event in the past decade, current acute illness or infection (e.g., COVID-19, cold, flu), or history of psychotic disorder or other major psychiatric illness except posttraumatic stress disorder (PTSD), depression, and anxiety which were exclusionary only if the conditions were so severe as to require hospitalization in the past 5 years. Before the scan day, patients were genotyped via saliva or blood for the Ala147Thr polymorphism in the *TSPO* gene (rs6971 polymorphism), which

is known to affect binding affinity for several TSPO radioligands, including [^{11}C]PBR28 (Owen et al., 2012, 2015). Individuals with the Ala/Ala or Ala/Thr genotypes (predicted high- and mixed-affinity binders, respectively) were included, and the genotype was modeled as a covariate in the statistical design. Individuals with the Thr/Thr genotype (predicted low-affinity binders) were excluded at the time of the screening and therefore not represented in our dataset. Medication exclusions included use of immunosuppressive medications such as prednisone or TNF blocking medications within the 2 weeks preceding the visit, routine use of benzodiazepines or any use in the past 2 weeks except clonazepam (Klonopin), lorazepam (Ativan), and alprazolam (Xanax), which have documented or predicted low affinity for TSPO (e.g., Kalk et al., 2013).

Before the scan, all participants underwent a history and physical examination by an experienced nurse practitioner to confirm PET-MRI safety. Participants answered several questionnaires and their height and weight were recorded. Immediately before neuroimaging, IV blood was drawn. Blood-based pregnancy testing (hCG) was performed on all individuals capable of becoming pregnant.

2.3. PET Imaging parameters

Our dual PET-MRI scanner consists of a 3-Tesla (3T) Siemens TIM Trio MRI (60 cm bore diameter) with 8-channel head coil and a photodiode-based high-resolution BrainPET head camera insert. The BrainPET prototype is a dedicated brain scanner that has 32 detector cassettes, each consisting of 6 detector blocks, each made up of a 12×12 array of lutetium oxyorthosilicate crystals (2.52 mm^3) read out by magnetic field-insensitive avalanche photodiodes. The transaxial and axial fields of view are 32 cm and 19.125 cm, respectively. The 3T MR system is equipped with the standard “TIM” (total imaging matrix) 32 RF channel receivers, accommodating up to 32 element array coils. [^{11}C]PBR28 radioligand was synthesized in-house using a Siemens Eclipse HP self-shielded 11 MeV cyclotron with single-beam extraction and a four position target-changer, by a procedure modified from the literature (for radioligand technical details see Imaizumi et al., 2007). During the PET scan, [^{11}C]PBR28 (up to 15 mCi, which is equivalent to ~3.7 mSv) was injected intravenously with a slow bolus over a ~30 s period (Debruyne et al., 2003). The catheter was then flushed post-injection with 0.9% sterile saline solution. Dynamic data was collected by the head PET camera over 90 min list mode and framed post-collection; concurrent high-resolution T1-weighted (MEMPRAGE) structural MRI images were collected for spatial registration of the PET data, as well as generation of attenuation correction maps (Izquierdo-Garcia et al., 2014) and scatter correction.

2.4. Blood collection

Immediately before [^{11}C]PBR28 injection and scanning, venous blood was collected from 11 PASC participants into a citrated vacutainer tube (BD 369714 light blue cap) (one participant was scanned when a study team member was out with COVID-19 and therefore blood was not collected). The citrate tube was gently upended 3x then left to sit at room temperature for 30 min, before centrifugation at 15 min x 3000 RCF x 20°C. Platelet-poor plasma (PPP) supernatant was pipetted into sterile 1.5 mL microtubes (Sarstedt Biosphere 72.703.217) and stored at −80°C. For analysis, these samples from the 11 PASC participants

were thawed on wet ice and 275 μL aliquots were pipetted into sterile SureSealTM 0.65 mL microfuge tubes (VWR Ward's Science 470228–444), marked with de-identified alphanumeric sequences, and sent overnight on dry ice to Eve Technologies (Calgary Canada) for analysis.

Three multiplex panels were conducted based upon previous PASC literature: vascular health, cytokine, and angiogenesis (e.g., Proal & VanElzakker, 2021; Klein et al., 2022; Patel et al., 2022). Analytes per multiplex were as follows: Vascular health (α2-macroglobulin, orosomucoid, CRP [C-reactive protein], fetuin A, fibrinogen, haptoglobin, sL-selectin, PF4 [platelet factor 4], pentraxin-2) (Millipore HCVD3MAG-67K Luminex magnetic bead panel); Cytokines (GM-CSF, IFNγ, IL-1β, IL-1RA, IL-2, IL-4, IL-5, IL-6, IL-8, IL-10, IL-12(p40), IL-12(p70), IL-13, MCP-1, TNFα) (Millipore HCYTA-60K Luminex magnetic bead panel); Angiogenesis (angiopoietin-2, BMP-9, EGF, endoglin, endothelin-1, FGF-1, FGF-2, follistatin, G-CSF, HB-EGF, HGF, IL-8, leptin, PLGF, VEGF-A, VEGF-C, VEGF-D) (Millipore HAGP1MAG-12K Luminex magnetic bead panel). Concentrations of these analytes were entered into a correlation matrix to test their relationship to extracted SUVR values and symptom measures in the PASC participants. Items from the vascular health panel are described in Box 1.

2.5. Behavioral measures

All 12 PASC and 43 eligible control participants were administered items from the Brief Pain Inventory (BPI) (Cleeland & Ryan, 1994) and the Beck Depression Inventory (BDI) (Beck et al., 1996).

PASC participants were screened to fulfill a modified myalgic encephalomyelitis/chronic fatigue syndrome (ME/CFS) International Consensus Criteria (ICC), and then on the day of the scan were asked to rate each ICC symptom's severity from 0 to 10. PASC individuals were also given a revised medical history questionnaire that asked about the history of several neurological or neuropsychiatric symptoms by naming a symptom then giving the option to either leave blank or select one of three options: 1) This was a problem for me before COVID-19, 2) This is a problem for me since I had COVID-19, or 3) This is a serious problem for me since I had COVID-19.

2.6. PET data processing

For the PASC versus control PET comparison, PET data processing was performed on a custom Linux-based pipeline used in several previous studies (e.g., Albrecht et al., 2019; Alshelh et al., 2021; Brusaferri et al., 2022; Loggia et al., 2015), including standard preprocessing and PET-MRI spatial registration to MNI (Montreal Neurological Institute) space.

Following data acquisition, several quality control steps were performed including by-participant visual inspection of detector blocks (Tayal et al., 2021), spatial registration, skull stripping, artifacts, and attenuation image map alignment. After normalizing radioactivity by injected dose by body weight, PET data were scatter- and attenuation-corrected using a custom MR-based method developed at the Martinos Center for Biomedical Imaging (Izquierdo-Garcia et al., 2014). For all participants, 30-minute static standardized uptake

value (SUV) PET images were reconstructed from data acquired ~60–90 min after the injection of the tracer. SUV maps were spatially normalized by nonlinear transformation into common MNI space and smoothed with an 8 mm FWHM (full-width half-maximum) Gaussian kernel. Standardized uptake value ratio (SUVR) images were then created by intensity-normalizing individual MNI-space SUV maps to cerebellum uptake, anatomically-defined by AAL (automatic anatomical labeling) atlas (Tzourio-Mazoyer et al., 2002). There were no group differences in cerebellum SUV in the 12 vs. 43 primary or the 11 vs. 11 validation analyses ($t(53) = 0.82$, $p = .42$; $t(10) = 0.85$, $p = .41$ respectively).

2.7. Statistical analysis

We conducted a primary unpaired (between groups) comparison including all available PET data (12 PASC vs. 43 control). Cerebellum-normalized, MNI-registered SUVR maps for each participant were entered into a general linear model, using the FEAT software tool (version 6.00, Woolrich et al., 2004) within FSL (FMRIB Software Library, Wellcome Centre). Nonparametric permutation inference of [^{11}C] PBR28 SUVR images was performed using FSL Randomise, with 5000 permutations (Winkler et al., 2014) and statistically controlling for sex and TSPO polymorphism. Cluster-correction was used to account for multiple comparisons, using a cluster-forming threshold of $Z = 2.3$ and cluster size of $p = .05$. Demographic and PET-relevant data comparisons for the primary analysis are shown in Table 1. Reflecting the sex distribution of PASC (Bai et al., 2022), there was a relatively high proportion of females (10) in the PASC group. While we did statistically control for sex in the primary analysis, we performed a second validation analysis using a paired approach in which each PASC participant was matched to a control participant for genotype, sex, and age ±5 years. Furthermore, we conducted an additional validation comparing only female PASC cases (n = 10) to female controls (n = 17) (Supplemental Fig. 1).

To test the relationship between SUVR and blood analyte or questionnaire data, simple Pearson's correlations were calculated. For these correlation analyses, we used the significant cluster that arose from the primary 12 PASC vs. 43 control comparison (see Results) and extracted each participant's average SUVR value from that cluster. For behavioral/demographic data, group statistical comparisons were performed using unpaired or paired Student's *t*-tests, Chi-square tests, or Pearson's correlation as appropriate, while BDI subscales were analyzed with a mixed-model ANOVA. Two-tailed *p*-values are reported in all cases. Cohen's *d* effect size for the primary analysis was calculated for selected voxels specified in Table 2.

3. Results

3.1. Imaging results: Voxelwise group differences

The voxelwise whole-brain comparison of PASC cases versus healthy controls revealed a significant increase in [^{11}C]PBR28 PET signal at the $Z = 2.3$ threshold. This increased PET signal spanned a wide swath of brain regions including midcingulate cortex, corpus callosum, thalamus, basal ganglia/striatum, subfornical organ, anterior cingulate cortex, medial frontal gyrus, and precentral gyrus (see Fig. 1 and Table 2), and is suggestive of glial

activation or neuroinflammation. There were no voxels with significantly greater SUVR values in the controls > PASC contrast.

In order to visualize data distribution, individual participants' data were extracted from the primary voxelwise analysis' significant cluster, and from a selection of atlas-defined anatomical regions that showed significant signal. The distribution pattern of extracted SUVR values showed that this effect was not driven by outliers or by hospitalized cases (Fig. 1B).

We conducted a paired validation analysis with individually matched PASC-control pairs and found a very similar PET signal pattern (Fig. 2).

3.2. Blood analyte measures and correlations

We found positive Pearson's *r* correlations between PET signal and the majority of analytes from the vascular disease multiplex panel (see Fig. 3, Table 3). Specifically, we found positive moderate to strong correlations between the PET signal extracted for each individual from the cluster derived from the voxelwise group comparison, and the concentrations of seven plasma vascular health-associated factors: fibrinogen ($r(9) = .80$, $p = .0032$), α2-macroglobulin ($r(9) = .73$, $p = .011$), orosomucoid (alpha-1-acid glycoprotein or AGP) ($r(9) = .69$, $p = .019$), fetuin A ($r(9) = .68$, $p = .022$), sL-selectin (soluble leukocyte selectin, or sCD62L) ($r(8) = .70$, $p = .025$), pentraxin-2 (serum amyloid P component, or SAP) ($r(9) = .66$, $p = .026$), and haptoglobin ($r(8) = .74$, $p = .015$). The haptoglobin scatterplot appeared to include a potential outlier. However, removing this participant from the analyses did not substantially affect significance, ($r(7) = .88$, $p = .0018$). The correlation with the C-reactive protein (CRP) was trending but not statistically significant ($r(8) = 0.61$, $p = .064$). In this case, the relevant scatterplot appeared to include one outlier, and another participant's levels were not detected by the assay. The CRP correlation remained non-significant after removing the potential outlier from the CRP analysis ($p > .4$). The high-end outlier in both haptoglobin and CRP analyses was the same participant, who was hospitalized during their acute COVID-19 illness. For both the sL-selectin and haptoglobin assays the same participant's levels were not detected by the respective assay, and platelet-factor 4 (PF4) was not detected by the assay in the majority of samples.

Cytokine concentrations from the 15-plex panel frequently correlated with one another but did not correlate with PET signal (Supplemental Fig. 2), which was our a-priori hypothesis (VanElzakker et al., 2019). Analytes from the angiogenesis 17-plex panel analytes also did not correlate with PET signal. We did not have strong a-priori hypotheses regarding correlations between blood analytes and self-reported symptoms.

3.3. Symptom severity and history

Response scores to the BPI severity item "Pain at its worst in the past 24 hrs" were higher in PASC ($M = 7.08$, $SD = 3.72$) versus controls ($M = 0.44$, $SD = 0.81$), $t(52) = 10.91$, $p < .001$, two-tailed, unequal variance. Mean scores from BPI-Interference subscale items were higher in PASC ($M = 21.75$, $SD = 15.42$) versus controls ($M = 0.90$, $SD = 0.31$), $t(51) = 9.21$, $p < .001$, two-tailed, unequal variance.

Mean total BDI scores were higher in cases ($M = 11.58$, $SD = 1.74$) versus controls ($M = 1.14$, $SD = 5.58$), $t(52) = 9.96$, $p < .001$, two-tailed, unequal variance. Mean depression severity according to the BDI was on average categorized as mild (10–18) in PASC and none-to-minimal (0–9) in controls. Two PASC cases met the threshold of moderate depression (19–29), with scores of 19 and 25. Of the 12 PASC cases, six reported that depression was not a problem, five reported "This is a problem for me since I had COVID-19" and one reported "This is a serious problem for me since I had COVID-19" about depression.

BDI responses can be divided into affective (mood-centered) versus somatic (body-centered) subscales. To better understand which questionnaire items were driving the higher BDI scores in PASC vs. controls, we conducted a 2×2 mixed model ANOVA with diagnosis (PASC, control) as the between-groups factor and BDI subscale (affective, somatic) as the within-subjects factor. This ANOVA revealed a significant interaction between diagnosis and BDI subscale $F(1,52) = 51.734$, $p < .001$, (partial $eta^2 = .499$, large effect size) driven by higher average item somatic subscale scores within the PASC group (Supplemental Table 1). There were also main effects of diagnosis $F(1,52) = 155.184$, $p < .001$ (consistent with the t-test) as well as a main effect of BDI subscale $F(1,52) = 54.236$, $p < .001$ in which average item score was higher in somatic versus affective subscales independent of diagnosis.

On the day of the scan, PASC participants self-reported the severity of each of the 21 ICC symptoms on a 0–10 scale (see Supplemental Fig. 3); all reported 5 out of 10 severity or greater on at least two of the eight ICC Neurological symptoms cluster items: headache, unrefreshing sleep, significant pain, short-term memory loss, difficulty processing information, sensory sensitivity, disturbed sleep pattern, and motor symptoms (e.g., twitching, poor coordination). Supplemental Fig. 3 depicts the six symptoms that overlapped between both the ICC scale (rating day-of-scan severity 0–10) and the medical history questionnaire (marking onset relative to acute COVID-19).

4. Discussion

We conducted PET neuroimaging and blood analyses in individuals with ongoing diverse symptoms that began with acute COVID-19 infection. The majority of PASC participants' acute COVID-19 illness did not require hospitalization. We found a significant increase in [^{11}C] PBR28 signal, an indicator of neuroinflammation, across a wide area of brain regions such as the midcingulate cortex, corpus callosum, thalamus, basal ganglia/striatum, subfornical organ, anterior cingulate cortex, medial frontal gyrus, and precentral gyrus.

Of note, one study reported increased TSPO signal in moderately depressed PASC participants, 45% (9 of 20) of which had pre-COVID depression (Braga et al., 2023). In contrast, in the current study's PASC cohort, the average depression score was mild, and no PASC participant reported a pre-COVID history of depression. Instead, they either denied depression being a problem for them (50%, 6 of 12) or reported that it was a new (~42%, 5 of 12) or serious new (~8%, 1 of 12) problem since COVID-19, and only 2 of 12 PASC participants were in the moderate depression severity range.

Importantly, in our study, we found that intensity of whole-brain PET signal showed significant positive correlations with blood measures related to vascular health (see Fig. 2 and Table 3). This is indirect evidence that differences in PET signal across brain structures (Fig. 1B) may partially reflect variance in vascular anatomy and perivascular immune penetration. To our knowledge, ours is the first study to provide direct evidence that processes related to neuroinflammation and vascular dysfunction are directly related in PASC.

As examples, fibrinogen and sL-selectin were two analytes from the vascular health multiplex panel that were significantly correlated with neuroinflammation-related PET signal. Elevated fibrinogen is associated with worse outcome in acute COVID-19 (Sui et al., 2021) and is not only associated with coagulation abnormalities in acute COVID-19 but also PASC (Pretorius et al., 2022; Sui et al., 2021). Related to neuroinflammation, fibrinogen persistently activates glia at the glymphatic (Mestre et al., 2017) perivascular spaces that surround neurovasculature (Davalos et al., 2012). Activated perivascular glia attract both glia from within the brain parenchyma and attract circulating immune factors to cross from neurovascular blood into brain. L-selectin (CD62L) is an adhesion molecule involved in attaching leukocytes (white blood cells) to vascular endothelium at sites of inflammation. Attraction of activated immune cells, inflammation of vascular endothelium, mobilization of glia, and activation of glia would each increase TSPO concentrations and therefore PET signal (as well as the symptoms associated with glial activation). The fact that these and other measures related to vascular dysfunction correlated with neuroinflammation provides evidence that the spatial pattern of PET signal in PASC vs. controls may reflect a vascular-related anatomical pattern that is likely to differ among patients. See Box 1 for further explanation of vascular analytes.

These vascular factors may penetrate into brain parenchyma via the perivascular spaces that line the neurovasculature and form the blood–brain barrier (Ineichen et al., 2022). During neuroinflammation, the blood–brain barrier becomes more permissive by opening up at the perivascular spaces, allowing circulating factors to affect the brain's glia (Galea, 2021). We found increased PET uptake in some regions that tend to have dilated perivascular spaces. For example, we found significantly increased PET signal especially within left lentiform nucleus of the basal ganglia. The basal ganglia are a group of subcortical nuclei with many small, thin blood vessels that are common sites of unique perivascular anatomy and enlarged/dilated perivascular spaces (Mestre et al., 2017; Rudie et al., 2018), and apparently-subclinical neurovascular abnormalities such as cerebral microhemorrhages (Viswanathan & Chabriat, 2006), both of which have been reported in acute COVID-19 autopsy (Kantonen et al., 2020). In neuroradiology, dilated perivascular spaces on the lenticulostriate arteries projecting into the basal ganglia are relatively common and referred to as "Type 1." Enlarged Type 1 perivascular spaces are sometimes seen in normal healthy aging but are associated with disease severity in some neurological conditions (Chan et al., 2021) and in one study were associated with sleep dysfunction in PASC (Del Brutto et al., 2022).

Within subcortical areas, some of the TSPO signal elevation pattern we measured also appears to be compatible with the location of the subfornical organ and the choroid plexus and ependymal glial cells at the roof of the third and floor of lateral ventricles, which

are circumventricular organs (CVOs). CVOs are dense with ACE2 receptors (Ong et al., 2022), highly vascularized, and (except for the subcommissural organ) feature fenestrated blood vessels that lack a complete blood—-brain barrier. This renders the glia near CVOs particularly vulnerable to being activated by blood-borne factors. We also detected elevated [^{11}C] PBR28 PET signal across cingulate and corpus callosum, a pattern that follows the anterior cerebral artery pericallosal branch. More posterior regions of cingulate are particularly highly vascularized (Vogt, 2019). Unlike the CVOs, but like the rest of the brain, these regions feature an intact blood-brain barrier. However, neurovascular endothelial cells are the blood-facing component of the blood–brain barrier and can be activated by circulating factors, in turn driving activation of glia (Kanda et al., 1995; Lécuyer et al., 2016; Pan et al., 2011). Furthermore, a reduced integrity of the blood–brain barrier, as observed during neuroinflammation (Galea, 2021), would likely contribute to this effect.

While our observational case-control study design cannot determine a causal relationship between neuroinflammation and vascular health, multiple potential non-mutually exclusive drivers (Proal & VanElzakker, 2021) of these effects are possible. Ongoing vascular-related problems and neuroinflammation may reflect lingering consequences from tissue injury during acute COVID-19. However most of our PASC participants did not report severe acute illness, and the acute COVID-19 illness that initiated their PASC was an average of 20.5 months prior to the scan visit. Under these circumstances, the ongoing objective neurological and vascular abnormalities may be more likely to reflect pre-COVID vulnerability factors and/or persistent stimulation by ongoing biological factors.

Previous studies have examined the contribution of other circulating factors in PASC. Vascular dysfunction may be consistent with the ongoing presence of fibrin-amyloid ‘microclots’ (Pretorius et al., 2022) or with neutrophil hyperactivation (Boribong et al., 2022) that have been reported in individuals with PASC. These factors may represent continuous provocation by uncleared viral reservoirs at least in some PASC patients (Proal et al., 2023; Proal & VanElzakker, 2021). SARS-CoV-2 RNA or protein has been identified in PASC tissue after acute COVID-19, and multiple research groups have identified SARS-CoV-2 proteins including spike in blood in a subset of PASC individuals up to 16 months after initial infection (Swank et al., 2023; Peluso et al., 2024). These proteins may have leaked into general circulation from a tissue reservoir site via extracellular vesicle transport (Craddock et al., 2023; Peluso et al., 2022). Given that the spike protein drives coagulation cascades (Zheng et al., 2021) and a profound inflammatory response (e. g., Boribong et al., 2022), future PASC studies should measure these variables together in PASC cases versus COVID-recovered controls to better understand how they may be related to neuroinflammation and ongoing symptoms. Better understanding of these potential sources of neuroinflammation would be important for guiding related treatments and clinical trials.

4.1. Limitations

The current study compared 12 PASC patients to 43 controls, the majority of whom (34) were scanned pre-pandemic, the rest of whom tested negative for SARS-CoV-2 antibodies. Future studies should also recruit a specific well-defined PASC phenotype but increase the number of PASC participants, and should also compare PASC to COVID-19-recovered

controls, including a direct comparison of circulating vascular measures. While there was a higher proportion of female participants in the PASC group, we statistically controlled for sex in the primary analysis, and conducted a paired validation analysis in which PASC participants were directly matched for sex, genotype, and age (±5yrs). Furthermore, we conducted a confirmatory unpaired analysis comparing only female PASC cases to only female controls and found a very similar pattern (see Supplemental data).

While the TSPO-targeting radioligand [^{11}C]PBR28 is a widely used measure in studies of neuroinflammation, the specific function of TSPO is an area of ongoing study. TSPO is involved in a number of biological functions including the transport of cholesterol molecule across mitochondrial membranes, which is the rate limiting step for the process of steroidogenesis. However, TSPO is perhaps best known for its role as a marker of neuroinflammation, given the colocalization of its upregulation with activated glia (Papadopoulos et al., 2006) and/or increased glial cell density (Nutma et al., 2023). In a non-mutually exclusive fashion, increased TSPO may reflect various activation states of glial cell types such as microglia and astrocytes (Paolicelli et al., 2022), density of glial cells (some of which are motile (Smolders et al., 2019)), peripheral immune cells penetrating into brain, or inflammatory activation of neurovascular endothelial cells (Guilarte et al., 2022). Therefore the exact biological driver of the observed increased PET signal in PASC remains to be fully elucidated. However, the observed correlations between PET signal and the blood concentration of vascular markers suggests that peripheral immune cells infiltrating the parenchyma, possibly enabled by a more permeable blood–brain barrier, as well as endothelial activation may at least contribute to our observation.

Kinetic modeling using radiometabolite-corrected arterial input function, which is considered by many to be the gold-standard for PET radioligand signal quantification, was not included in the current study because arterial line data were available only in a small subset of participants, insufficient for a comparison. We instead used a simplified, semiquantitative ratio metric, SUVR. It is worth mentioning that several studies have now shown that for TSPO radioligands V_T (distribution volume) is a measure that is very highly variable across individuals, and this variability (which may be induced by a variety of factors) needs to be controlled for in order to unveil genuine physiological effects (e.g., Turkheimer et al., 2015) This is typically achieved by normalizing the PET signal, i.e. by dividing either V_T or SUV for the target region by that of a pseudoreference region or the whole brain (Lyoo et al., 2015; Turkheimer et al., 2015) to create, respectively, DVR or SUVR. For instance, SUVR allowed detection of differences in [^{11}C]PBR28 binding between patients with Alzheimer's disease and healthy controls with greater sensitivity than V_T (Lyoo et al., 2015). While SUVR is typically not well correlated with V_T, our group has shown in multiple studies and in multiple patient groups that it highly correlates with DVR (Albrecht et al., 2018, 2021; Alshelh et al., 2020). Nonetheless, while we believe this approach to be valuable, future studies will need to provide further validation for the use of semiquantitative ratio metrics in PASC studies, and to guide the choice of optimal pseudoreference regions. In this study we used cerebellum, which is the region most commonly used in studies with second-generation TSPO ligand to date (e.g. Kagitani-Shimono et al., 2021; López-Picón et al., 2022; Lyoo et al., 2015; Saleem et al., 2023; Schoenberg et al., 2023). There have been conflicting reports of cerebellar hypometabolism

in PASC patients using [^{18}F]FDG (Goehringer et al., 2023; Guedj et al., 2021). However, Braga et al. (2023) used arterial-line-based kinetic modeling and also found no difference in [^{11}C]PBR28 cerebellar uptake between PASC and controls, providing support for the validity of using this structure as a pseudoreference region. Validation of an arterial line-independent approach may be particularly important in PASC given the likely centrality of vascular problems and evidence for COVID-19 effects on arterial stiffness, Raynaud's phenomenon, and hypercoagulability, rendering arterial line placement inadvisable for some PASC study participants.

Supplementary Material

Refer to Web version on PubMed Central for supplementary material.

Acknowledgments

Funding provided by PolyBio Research Foundation. Additional funding for control scans, Martinos Center infrastructure, and author effort provided by NIH grants 3R01DA047088-05S1, 1R21NS130283-01A1, 1S10RR023401, 1S10RR019307, and 1S10RR023043. Thanks to Brent Vogt PhD and Amy Proal PhD for helpful feedback on earlier versions of the manuscript, the Martinos Center PET and radiochemistry team, and especially the study participants.

Data availability

Data will be made available on request.

References

Ajčević M, Iscra K, Furlanis G, Michelutti M, Miladinović A, Buoite Stella A, Ukmar M, Cova MA, Accardo A, Manganotti P, 2023. Cerebral hypoperfusion in post-COVID-19 cognitively impaired subjects revealed by arterial spin labeling MRI. Sci. Rep 13 (1), Article 1. 10.1038/s41598-023-32275-3.

Albrecht DS, Granziera C, Hooker JM, Loggia ML, 2016. In Vivo Imaging of Human Neuroinflammation. ACS Chem. Nerosci 7 (4), 470–483. 10.1021/acschemneuro.6b00056.

Albrecht DS, Normandin MD, Shcherbinin S, Wooten DW, Schwarz AJ, Zürcher NR, Barth VN, Guehl NJ, Akeju O, Atassi N, Veronese M, Turkheimer F, Hooker JM, Loggia ML, 2018. Pseudoreference Regions for Glial Imaging with 11C-PBR28: Investigation in 2 Clinical Cohorts. J. Nucl. Med 59 (1), 107–114. 10.2967/jnumed.116.178335. [PubMed: 28818984]

Albrecht DS, Forsberg A, Sandstrom A, Bergan C, Kadetoff D, Protsenko E, Lampa J, Lee YC, Olgart Höglund C, Catana C, Cervenka S, Akeju O, Lekander M, Cohen G, Halldin C, Taylor N, Kim M, Hooker JM, Edwards RR, Loggia ML, 2019. Brain glial activation in fibromyalgia—A multi-site positron emission tomography investigation. Brain Behav. Immun 75, 72–83. 10.1016/j.bbi.2018.09.018. [PubMed: 30223011]

Albrecht DS, Kim M, Akeju O, Torrado-Carvajal A, Edwards R, Zhang Y, Bergan C, Protsenko E, Kucyi A, Wasan A, Hooker J, Napadow V, Loggia M, 2021. The neuroinflammatory component of negative affect in patients with chronic pain. Mol. Psychiatry 26 (3), 864–874. 10.1038/s41380-019-0433-1. [PubMed: 31138890]

Alshelh Z, Albrecht DS, Bergan C, Akeju O, Clauw DJ, Conboy L, Edwards RR, Kim M, Lee YC, Protsenko E, Napadow V, Sullivan K, Loggia ML, 2020. In-vivo imaging of neuroinflammation in Veterans with Gulf War Illness. Brain Behav. Immun 87, 498–507. 10.1016/j.bbi.2020.01.020. [PubMed: 32027960]

Alshelh Z, Brusaferri L, Saha A, Morrissey E, Knight P, Kim M, Zhang Y, Hooker JM, Albrecht D, Torrado-Carvajal A, Placzek MS, Akeju O, Price J, Edwards RR, Lee J, Sclocco R, Catana C,

Napadow V, Loggia ML, 2021. Neuroimmune signatures in chronic low back pain subtypes. Brain 145(3), Article 3. 10.1093/brain/awab336.

Bai F, Tomasoni D, Falcinella C, Barbanotti D, Castoldi R, Mulè G, Augello M, Mondatore D, Allegrini M, Cona A, Tesoro D, Tagliaferri G, Viganò O, Suardi E, Tincati C, Beringheli T, Varisco B, Battistini CL, Piscopo K, Monforte AD, 2022. Female gender is associated with long COVID syndrome: A prospective cohort study. Clin. Microbiol. Infect 28 (4), 611.e9–611.e16. 10.1016/j.cmi.2021.11.002.

Barrientos RM, Higgins EA, Biedenkapp JC, Sprunger DB, Wright-Hardesty KJ, Watkins LR, Rudy JW, Maier SF, 2006. Peripheral infection and aging interact to impair hippocampal memory consolidation. Neurobiol. Aging 27 (5), 723–732. 10.1016/j.neurobiolaging.2005.03.010. [PubMed: 15893410]

Beck AT, Steer RA, Ball R, Ranieri W, 1996. Comparison of Beck Depression Inventories -IA and -II in psychiatric outpatients. J. Pers. Assess 67 (3), 588–597. 10.1207/s15327752jpa6703_13. [PubMed: 8991972]

Berkman JM, Rosenthal JA, Saadi A, 2021. Carotid Physiology and Neck Restraints in Law Enforcement: Why Neurologists Need to Make Their Voices Heard. JAMA Neurol. 78 (3), 267–268. 10.1001/jamaneurol.2020.4669. [PubMed: 33369628]

Boribong BP, LaSalle TJ, Bartsch YC, Ellett F, Loiselle ME, Davis JP, Gonye ALK, Sykes DB, Hajizadeh S, Kreuzer J, Pillai S, Haas W, Edlow AG, Fasano A, Alter G, Irimia D, Sade-Feldman M, Yonker LM, 2022. Neutrophil profiles of pediatric COVID-19 and multisystem inflammatory syndrome in children. Cell Reports Medicine 3 (12), 100848. 10.1016/j.xcrm.2022.100848.

Braga J, Lepra M, Kish SJ, Rusjan PM, Nasser Z, Verhoeff N, Vasdev N, Bagby M, Boileau I, Husain MI, Kolla N, Garcia A, Chao T, Mizrahi R, Faiz K, Vieira EL, & Meyer JH, 2023. Neuroinflammation After COVID-19 With Persistent Depressive and Cognitive Symptoms. JAMA Psychiat. 80 (8), 787–795. 10.1001/jamapsychiatry.2023.1321.

Brusaferri L, Alshelh Z, Martins D, Kim M, Weerasekera A, Housman H, Morrissey EJ, Knight PC, Castro-Blanco KA, Albrecht DS, Tseng C-E, Zürcher NR, Ratai E-M, Akeju O, Makary MM, Catana C, Mercaldo ND, Hadjikhani N, Veronese M, Loggia ML, 2022. The pandemic brain: Neuroinflammation in non-infected individuals during the COVID-19 pandemic. Brain Behav. Immun 102, 89–97. 10.1016/j.bbi.2022.02.018. [PubMed: 35181440]

Cabezas R, Ávila M, Gonzalez J, El-Bachá RS, Báez E, García-Segura LM, Jurado Coronel JC, Capani F, Cardona-Gomez GP, Barreto GE, 2014. Astrocytic modulation of blood brain barrier: Perspectives on Parkinson's disease. Front. Cell. Neurosci 8. https://www.frontiersin.org/articles/10.3389/fncel.2014.00211.

Carruthers BM, van de Sande MI, De Meirleir KL, Klimas NG, Broderick G, Mitchell T, Staines D, Powles ACP, Speight N, Vallings R, Bateman L, Baumgarten-Austrheim B, Bell DS, Carlo-Stella N, Chia J, Darragh A, Jo D, Lewis D, Light AR, Stevens S, 2011. Myalgic encephalomyelitis: International Consensus Criteria. J. Intern. Med 270 (4), Article 4. 10.1111/j.1365-2796.2011.02428.x.

Centers for Disease Control and Prevention. (2022). Long COVID or Post-COVID Conditions. https://www.cdc.gov/coronavirus/2019-ncov/long-term-effects/index.html.

Chan ST, Mercaldo ND, Ravina B, Hersch SM, & Rosas HD (2021). Association of Dilated Perivascular Spaces and Disease Severity in Patients With Huntington Disease. Neurology, 96(6), Article 6. 10.1212/WNL.0000000000011121.

Chekol Abebe E, Tilahun Muche Z, Behaile T/Mariam A, Mengie Ayele T, Mekonnen Agidew M, Teshome Azezew M, Abebe Zewde E, Asmamaw Dejenie T, Asmamaw Mengstie M, 2022. The structure, biosynthesis, and biological roles of fetuin-A: A review. Front. Cell Dev. Biol 10, 945287. 10.3389/fcell.2022.945287.

Cleeland CS, Ryan KM, 1994. Pain assessment: Global use of the Brief Pain Inventory. Ann. Acad. Med. Singapore 23 (2), 129–138. [PubMed: 8080219]

Craddock V, Mahajan A, Spikes L, Krishnamachary B, Ram AK, Kumar A, Chen L, Chalise P, Dhillon NK, 2023. Persistent circulation of soluble and extracellular vesicle-linked Spike protein in individuals with postacute sequelae of COVID-19. J. Med. Virol 95 (2), e28568.

Dantzer R, Kelley KW, 2007. Twenty Years of Research on Cytokine-Induced Sickness Behavior. Brain Behav. Immun 21 (2), 153–160. 10.1016/j.bbi.2006.09.006. [PubMed: 17088043]

Davalos D, Kyu Ryu J, Merlini M, Baeten KM, Le Moan N, Petersen MA, Deerinck TJ, Smirnoff DS, Bedard C, Hakozaki H, Gonias Murray S, Ling JB, Lassmann H, Degen JL, Ellisman MH, Akassoglou K, 2012. Fibrinogen-induced perivascular microglial clustering is required for the development of axonal damage in neuroinflammation. Nat. Commun 3, 1227. 10.1038/ncomms2230. [PubMed: 23187627]

Davis HE, Assaf GS, McCorkell L, Wei H, Low RJ, Re'em Y, Redfield S, Austin JP, & Akrami A, 2021. Characterizing long COVID in an international cohort: 7 months of symptoms and their impact. EClinicalMedicine 38, 101019. 10.1016/j.eclinm.2021.101019.

Debruyne JC, Versijpt J, Van Laere KJ, De Vos F, Keppens J, Strijckmans K, Achten E, Slegers G, Dierckx RA, Korf J, De Reuck JL, 2003. PET visualization of microglia in multiple sclerosis patients using [11C]PK11195. Eur. J. Neurol 10(3), Article 3 10.1046/j.1468-1331.2003.00571.x.

Del Brutto OH, Mera RM, Costa AF, Rumbea DA, Recalde BY, Castillo PR, 2022. Long coronavirus disease-related persistent poor sleep quality and progression of enlarged perivascular spaces. A longitudinal study. Sleep zsac168. 10.1093/sleep/zsac168.

Douaud G, Lee S, Alfaro-Almagro F, Arthofer C, Wang C, McCarthy P, Lange F, Andersson JLR, Griffanti L, Duff E, Jbabdi S, Taschler B, Keating P, Winkler AM, Collins R, Matthews PM, Allen N, Miller KL, Nichols TE, & Smith SM (2022). SARS-CoV-2 is associated with changes in brain structure in UK Biobank. Nature, 604(7907), Article 7907. 10.1038/s41586-022-04569-5.

Galea I (2021). The blood–brain barrier in systemic infection and inflammation. Cellular & Molecular Immunology, 18(11), Article 11. 10.1038/s41423-021-00757-x.

Doni A, Mantovani A, Bottazzi B, Russo RC, 2021. PTX3 Regulation of Inflammation, Hemostatic Response, Tissue Repair, and Resolution of Fibrosis Favors a Role in Limiting Idiopathic Pulmonary Fibrosis. Front. Immunol 12, 676702. 10.3389/fimmu.2021.676702.

Goehringer F, Bruyere A, Doyen M, Bevilacqua S, Charmillon A, Heyer S, Verger A, 2023. Brain 18F-FDG PET imaging in outpatients with post-COVID-19 conditions: Findings and associations with clinical characteristics. Eur. J. Nucl. Med. Mol. Imaging 50 (4), 1084–1089. 10.1007/s00259-022-06013-2. [PubMed: 36322190]

Graw JA, Yu B, Rezoagli E, Warren HS, Buys ES, Bloch DB, Zapol WM, 2017. Endothelial dysfunction inhibits the ability of haptoglobin to prevent hemoglobin-induced hypertension. Am. J. Phys. Heart Circ. Phys 312 (6), H1120–H1127. 10.1152/ajpheart.00851.2016.

Guedj E, Campion JY, Dudouet P, Kaphan E, Bregeon F, Tissot-Dupont H, Guis S, Barthelemy F, Habert P, Ceccaldi M, Million M, Raoult D, Cammilleri S, Eldin C, 2021. 18F-FDG brain PET hypometabolism in patients with long COVID. Eur. J. Nucl. Med. Mol. Imaging 48 (9), 2823–2833. 10.1007/s00259-021-05215-4. [PubMed: 33501506]

Guilarte TR, Rodichkin AN, McGlothan JL, De La Rocha AMA, Azzam DJ, 2022. Imaging neuroinflammation with TSPO: A new perspective on the cellular sources and subcellular localization. Pharmacol. Ther 234, 108048 10.1016/j.pharmthera.2021.108048.

Imaizumi M, Kim H-J, Zoghbi SS, Briard E, Hong J, Musachio JL, Ruetzler C, Chuang D-M, Pike VW, Innis RB, Fujita M, 2007. PET imaging with [11C] PBR28 can localize and quantify upregulated peripheral benzodiazepine receptors associated with cerebral ischemia in rat. Neurosci. Lett 411 (3), 200–205. 10.1016/j.neulet.2006.09.093. [PubMed: 17127001]

Ineichen BV, Okar SV, Proulx ST, Engelhardt B, Lassmann H, Reich DS, 2022. Perivascular spaces and their role in neuroinflammation. Neuron 110 (21), 3566–3581. 10.1016/j.neuron.2022.10.024. [PubMed: 36327898]

Ivetic A, Hoskins Green HL, Hart SJ, 2019. L-selectin: A Major Regulator of Leukocyte Adhesion. Migration and Signaling. Frontiers in Immunology 10, 1068. 10.3389/fimmu.2019.01068. [PubMed: 31139190]

Izquierdo-Garcia D, Hansen AE, Förster S, Benoit D, Schachoff S, Fürst S, Chen KT, Chonde DB, Catana C, 2014. An SPM8-based Approach for Attenuation Correction Combining Segmentation and Non-rigid Template Formation: Application to Simultaneous PET/MR Brain Imaging. Journal of Nuclear Medicine : Official Publication, Society of. Nuclear Medicine 55 (11), Article 11. 10.2967/jnumed.113.136341.

Kagitani-Shimono K, Kato H, Kuwayama R, Tominaga K, Nabatame S, Kishima H, Hatazawa J, Taniike M, 2021. Clinical evaluation of neuroinflammation in child-onset focal epilepsy:

A translocator protein PET study. J. Neuroinflammation 18, 8. 10.1186/s12974-020-02055-1. [PubMed: 33407581]

Kalk N. j., Owen D. r., Tyacke R. j., Reynolds R, Rabiner E. a., Lingford-hughes A. r., & Parker C. a., 2013. Are prescribed benzodiazepines likely to affect the availability of the 18 kDa translocator protein (TSPO) in PET studies? Synapse 67 (12), 909–912. 10.1002/syn.21681. [PubMed: 23666806]

Kanda T, Yamawaki M, Ariga T, & Yu RK (1995). Interleukin 1 beta up-regulates the expression of sulfoglucuronosyl paragloboside, a ligand for L-selectin, in brain microvascular endothelial cells. Proceedings of the National Academy of Sciences of the United States of America, 92(17), 7897–7901. [PubMed: 7544008]

Kantonen J, Mahzabin S, Mäyränpää MI, Tynninen O, Paetau A, Andersson N, Sajantila A, Vapalahti O, Carpén O, Kekäläinen E, Kantele A, Myllykangas L, 2020. Neuropathologic features of four autopsied COVID-19 patients. Brain Pathol. 30 (6), 1012–1016. 10.1111/bpa.12889. [PubMed: 32762083]

Klein J, Wood J, Jaycox J, Lu P, Dhodapkar RM, Gehlhausen JR, Tabachnikova A, Tabacof L, Malik AA, Kamath K, Greene K, Monteiro VS, Peña-Hernandez M, Mao T, Bhattacharjee B, Takahashi T, Lucas C, Silva J, Mccarthy D, … Iwasaki A (2022). (Pre-print) Distinguishing features of Long COVID identified through immune profiling. medRxiv. 10.1101/2022.08.09.22278592.

Lécuyer M-A, Kebir H, Prat A, 2016. Glial influences on BBB functions and molecular players in immune cell trafficking. Biochim. Biophys. Acta (BBA) - Mol. Basis Dis. 1862 (3), 472–482. 10.1016/j.bbadis.2015.10.004.

Lesteberg KE, Araya P, Waugh KA, Chauhan L, Espinosa JM, Beckham JD, 2023. Severely ill and high-risk COVID-19 patients exhibit increased peripheral circulation of CD62L+ and perforin+ T cells. Front. Immunol 14. https://www.frontiersin.org/articles/10.3389/fimmu.2023.1113932.

Li H, Sun J, Nan G, 2019. Orosomucoid and Cerebral Stroke: A Mini Review. Biomed. J. Sci. Tech. Res. (BJSTR) 13 (5). 10.26717/BJSTR.2019.13.002468.

Lindgren N, Tuisku J, Vuoksimaa E, Helin S, Karrasch M, Marjamäki P, Kaprio J, Rinne JO, 2020. Association of neuroinflammation with episodic memory: A [11C] PBR28 PET study in cognitively discordant twin pairs. Brain. Communications 2 (1), fcaa024. 10.1093/braincomms/fcaa024.

Líška D, Liptaková E, Babičová A, Batalik L, Baňárová PS, & Dobrodenková S (2022). What is the quality of life in patients with long COVID compared to a healthy control group? Frontiers in Public Health, 10. https://www.frontiersin.org/articles/10.3389/fpubh.2022.975992.

Loggia ML, Chonde DB, Akeju O, Arabasz G, Catana C, Edwards RR, Hill E, Hsu S, Izquierdo-Garcia D, Ji R-R, Riley M, Wasan AD, Zürcher NR, Albrecht DS, Vangel MG, Rosen BR, Napadow V, Hooker JM, 2015. Evidence for brain glial activation in chronic pain patients. Brain 138 (3), 604–615. 10.1093/brain/awu377. [PubMed: 25582579]

López-Picón FR, Keller T, Bocancea D, Helin JS, Krzyczmonik A, Helin S, Damont A, Dollé F, Rinne JO, Haaparanta-Solin M, Solin O, 2022. Direct Comparison of [18F]F-DPA with [18F]DPA-714 and [11C]PBR28 for Neuroinflammation Imaging in the same Alzheimer's Disease Model Mice and Healthy Controls. Mol. Imag. Biol 24 (1), 157–166. 10.1007/s11307-021-01646-5.

Luyendyk JP, Schoenecker JG, Flick MJ, 2019. The multifaceted role of fibrinogen in tissue injury and inflammation. Blood 133 (6), 511–520. 10.1182/blood-2018-07-818211. [PubMed: 30523120]

Lyoo CH, Ikawa M, Liow J-S, Zoghbi SS, Morse C, Pike VW, Fujita M, Innis RB, Kreisl WC, 2015. Cerebellum can serve as a pseudo-reference region in Alzheimer's disease to detect neuroinflammation measured with PET radioligand binding to translocator protein (TSPO). Journal of Nuclear Medicine : Official Publication, Society of Nuclear Medicine 56 (5), 701–706. 10.2967/jnumed.114.146027. [PubMed: 25766898]

Ma Y, Deng J, Liu Q, Du M, Liu M, Liu J, 2023. Long-Term Consequences of Asymptomatic SARS-CoV-2 Infection: A Systematic Review and Meta-Analysis. Int. J. Environ. Res. Public Health 20 (2), 1613. 10.3390/ijerph20021613. [PubMed: 36674367]

Mestre H, Kostrikov S, Mehta RI, & Nedergaard M (2017). Perivascular Spaces, Glymphatic Dysfunction, and Small Vessel Disease. Clinical Science (London, England : 1979), 131(17), 2257–2274. 10.1042/CS20160381. [PubMed: 28798076]

Muczynski V, Aymé G, Regnault V, Vasse M, Borgel D, Legendre P, Bazaa A, Harel A, Loubière C, Lenting PJ, Denis CV, Christophe OD, 2017. Complex formation with pentraxin-2 regulates factor X plasma levels and macrophage interactions. Blood 129 (17), 2443–2454. 10.1182/blood-2016-06-724351. [PubMed: 28213380]

National Center for Health Statistics. (2023). U.S. Census Bureau, Household Pulse Survey, 2022–2023. Long COVID. https://www.cdc.gov/nchs/covid19/pulse/long-covid.htm.

Nutma E, Fancy N, Weinert M, Tsartsalis S, Marzin MC, Muirhead RCJ, Falk I, Breur M, de Bruin J, Hollaus D, Pieterman R, Anink J, Story D, Chandran S, Tang J, Trolese MC, Saito T, Saido TC, Wiltshire KH, … Owen DR (2023). Translocator protein is a marker of activated microglia in rodent models but not human neurodegenerative diseases. Nature Communications, 14(1), Article 1. 10.1038/s41467-023-40937-z.

Ong W-Y, Satish RL, Herr DR, 2022. ACE2, Circumventricular Organs and the Hypothalamus, and COVID-19. NeuroMol. Med 24 (4), 363–373. 10.1007/s12017-022-08706-1.

Owen DR, Yeo AJ, Gunn RN, Song K, Wadsworth G, Lewis A, Rhodes C, Pulford DJ, Bennacef I, Parker CA, StJean PL, Cardon LR, Mooser VE, Matthews PM, Rabiner EA, Rubio JP, 2012. An 18-kDa Translocator Protein (TSPO) polymorphism explains differences in binding affinity of the PET radioligand PBR28. J. Cereb. Blood Flow Metab. 32 (1), 1–5. 10.1038/jcbfm.2011.147. [PubMed: 22008728]

Owen DR, Guo Q, Rabiner EA, Gunn RN, 2015. The impact of the rs6971 polymorphism in TSPO for quantification and study design. Clinical and Translational Imaging 3 (6), 417–422. 10.1007/s40336-015-0141-z.

Pan W, Stone KP, Hsuchou H, Manda VK, Zhang Y, Kastin AJ, 2011. Cytokine Signaling Modulates Blood-Brain Barrier Function. Curr. Pharm. Des 17 (33), 3729–3740. [PubMed: 21834767]

Pannell M, Economopoulos V, Wilson TC, Kersemans V, Isenegger PG, Larkin JR, Smart S, Gilchrist S, Gouverneur V, Sibson NR, 2020. Imaging of translocator protein upregulation is selective for pro-inflammatory polarized astrocytes and microglia. Glia 68 (2), 280–297. 10.1002/glia.23716. [PubMed: 31479168]

Paolicelli RC, Sierra A, Stevens B, Tremblay M-E, Aguzzi A, Ajami B, Amit I, Audinat E, Bechmann I, Bennett M, Bennett F, Bessis A, Biber K, Bilbo S, Blurton-Jones M, Boddeke E, Brites D, Brône B, Brown GC, Wyss-Coray T, 2022. Microglia states and nomenclature: A field at its crossroads. Neuron 110 (21), 3458–3483. 10.1016/j.neuron.2022.10.020. [PubMed: 36327895]

Papadopoulos V, Baraldi M, Guilarte TR, Knudsen TB, Lacapère J-J, Lindemann P, Norenberg MD, Nutt D, Weizman A, Zhang M-R, Gavish M, 2006. Translocator protein (18kDa): New nomenclature for the peripheral-type benzodiazepine receptor based on its structure and molecular function. Trends Pharmacol. Sci 27 (8), 402–409. 10.1016/j.tips.2006.06.005. [PubMed: 16822554]

Patel MA, Knauer MJ, Nicholson M, Daley M, Van Nynatten LR, Martin C, Patterson EK, Cepinskas G, Seney SL, Dobretzberger V, Miholits M, Webb B, Fraser DD, 2022. Elevated vascular transformation blood biomarkers in Long-COVID indicate angiogenesis as a key pathophysiological mechanism. Mol. Med 28 (1), 122. 10.1186/s10020-022-00548-8. [PubMed: 36217108]

Peluso MJ, Deeks SG, Mustapic M, Kapogiannis D, Henrich TJ, Lu S, Goldberg SA, Hoh R, Chen JY, Martinez EO, Kelly JD, Martin JN, Goetzl EJ, 2022. SARS-CoV-2 and Mitochondrial Proteins in Neural-Derived Exosomes of COVID-19. Ann. Neurol 91 (6), 772–781. 10.1002/ana.26350. [PubMed: 35285072]

Peluso MJ, Swank ZN, Goldberg SA, Lu S, Dalhuisen T, Borberg E, Senussi Y, Luna MA, Chang Song C, Clark A, Zamora A, Lew M, Viswanathan B, Huang B, Anglin K, Hoh R, Hsue PY, Durstenfeld MS, Spinelli MA, Glidden DV, … Martin JN (2024). Plasma-based antigen persistence in the post-acute phase of COVID-19. The Lancet. Infectious diseases, S1473–3099(24)00211–1. Advance online publication. 10.1016/S1473-3099(24)00211-1.

Pretorius E, Venter C, Laubscher GJ, Kotze MJ, Oladejo SO, Watson LR, Rajaratnam K, Watson BW, Kell DB, 2022. Prevalence of symptoms, comorbidities, fibrin amyloid microclots and platelet pathology in individuals with Long COVID/Post-Acute Sequelae of COVID-19 (PASC). Cardiovasc. Diabetol 21 (1), 148. 10.1186/s12933-022-01579-5. [PubMed: 35933347]

Proal AD, VanElzakker MB, 2021. Long COVID or Post-acute Sequelae of COVID-19 (PASC): An Overview of Biological Factors That May Contribute to Persistent Symptoms. Front. Microbiol 12, 698169 10.3389/fmicb.2021.698169.

Proal AD, VanElzakker MB, Aleman S, Bach K, Boribong BP, Buggert M, Cherry S, Chertow DS, Davies HE, Dupont CL, Deeks SG, Eimer W, Ely EW, Fasano A, Freire M, Geng LN, Griffin DE, Henrich TJ, Iwasaki A, Wherry EJ, 2023. SARS-CoV-2 reservoir in post-acute sequelae of COVID-19 (PASC). Nat. Immunol 1–12 10.1038/s41590-023-01601-2.

Rudie JD, Rauschecker AM, Nabavizadeh SA, Mohan S, 2018. Neuroimaging of Dilated Perivascular Spaces: From Benign and Pathologic Causes to Mimics. Journal of Neuroimaging : Official Journal of the American Society of Neuroimaging 28 (2), 139–149. 10.1111/jon.12493.

Saleem A, Shah SIA, Mangar SA, Coello C, Wall MB, Rizzo G, Jones T, Price PM, 2023. Cognitive Dysfunction in Patients Treated with Androgen Deprivation Therapy: A Multimodality Functional Imaging Study to Evaluate Neuroinflammation. Prostate Cancer 2023, 6641707. 10.1155/2023/6641707.

Schoenberg PLA, Song AK, Mohr EM, Rogers BP, Peterson TE, Murphy BA, 2023. Increased microglia activation in late non-central nervous system cancer survivors links to chronic systemic symptomatology. Hum. Brain Mapp. 44 (17), 6001–6019. 10.1002/hbm.26491. [PubMed: 37751068]

Seekamp A, van Griensven M, Hildebrandt F, Brauer N, Jochum M, Martin M, 2001. The effect of trauma on neutrophil L-selectin expression and sL-selectin serum levels. Shock (augusta, Ga.) 15 (4), 254–260. 10.1097/00024382-200115040-00002. [PubMed: 11303723]

Smolders S-M-T, Kessels S, Vangansewinkel T, Rigo J-M, Legendre P, Brône B, 2019. Microglia: Brain cells on the move. Prog. Neurobiol 178, 101612 10.1016/j.pneurobio.2019.04.001.

Sui J, Noubouossie DF, Gandotra S, Cao L, 2021. Elevated Plasma Fibrinogen Is Associated With Excessive Inflammation and Disease Severity in COVID-19 Patients. In: Frontiers in Cellular and Infection Microbiology, p. 11.

Swank Z, Senussi Y, Manickas-Hill Z, Yu XG, Li JZ, Alter G, Walt DR, 2023. Persistent Circulating Severe Acute Respiratory Syndrome Coronavirus 2 Spike Is Associated With Post-acute Coronavirus Disease 2019 Sequelae. Clin. Infect. Dis 76 (3), e487–e490. 10.1093/cid/ciac722. [PubMed: 36052466]

Tayal S, Ali A, Kumar V, Jha AK, Gandhi A, 2021. Importance of Understanding and Analyzing Daily Quality Assurance Test of Positron Emission Tomography/Computed Tomography Equipment in Minimizing the Downtime of Equipment in Remote Places. Indian Journal of Nuclear Medicine : IJNM : the Official Journal of the Society of Nuclear Medicine, India 36 (2), 179–182. 10.4103/ijnm.IJNM_196_20. [PubMed: 34385790]

Turkheimer FE, Rizzo G, Bloomfield PS, Howes O, Zanotti-Fregonara P, Bertoldo A, Veronese M, 2015. The methodology of TSPO imaging with positron emission tomography. Biochem. Soc. Trans 43 (4), 586–592. 10.1042/BST20150058. [PubMed: 26551697]

Tzourio-Mazoyer N, Landeau B, Papathanassiou D, Crivello F, Etard O, Delcroix N, Mazoyer B, Joliot M, 2002. Automated anatomical labeling of activations in SPM using a macroscopic anatomical parcellation of the MNI MRI single-subject brain. Neuroimage 15 (1), 273–289. 10.1006/nimg.2001.0978. [PubMed: 11771995]

Vandooren J, Itoh Y, 2021. Alpha-2-Macroglobulin in Inflammation, Immunity and Infections. Front. Immunol 12, 803244. 10.3389/fimmu.2021.803244.

VanElzakker MB, Brumfield SA, Lara Mejia PS, 2019. Neuroinflammation and Cytokines in Myalgic Encephalomyelitis/Chronic Fatigue Syndrome (ME/CFS): A Critical Review of Research Methods. Front. Neurol 9, 1033. 10.3389/fneur.2018.01033. [PubMed: 30687207]

Viswanathan A, Chabriat H, 2006. Cerebral Microhemorrhage. Stroke 37 (2), 550–555. 10.1161/01.STR.0000199847.96188.12. [PubMed: 16397165]

Vogt BA (2019). Chapter 1 - The cingulate cortex in neurologic diseases: History, Structure, Overview. In Vogt BA (Ed.), Handbook of Clinical Neurology (Vol. 166, pp. 3–21). Elsevier. 10.1016/B978-0-444-64196-0.00001-7. [PubMed: 31731918]

Winkler AM, Ridgway GR, Webster MA, Smith SM, Nichols TE, 2014. Permutation inference for the general linear model. Neuroimage 92 (100), 381–397. 10.1016/j.neuroimage.2014.01.060. [PubMed: 24530839]

Woolrich MW, Behrens TEJ, Beckmann CF, Jenkinson M, Smith SM, 2004. Multilevel linear modelling for FMRI group analysis using Bayesian inference. Neuroimage 21 (4), 1732–1747. 10.1016/j.neuroimage.2003.12.023. [PubMed: 15050594]

World Health Organization. (2021). A clinical case definition of post COVID-19 condition by a Delphi consensus, 6 October 2021. https://www.who.int/publications/i/item/WHO-2019-nCoV-Post_COVID-19_condition-Clinical_case_definition-2021.1.

Xie Y, Xu E, Bowe B, Al-Aly Z, 2022. Long-term cardiovascular outcomes of COVID-19. Nat. Med 28 (3), Article 3. 10.1038/s41591-022-01689-3.

Xu E, Xie Y, Al-Aly Z, 2022. Long-term neurologic outcomes of COVID-19. Nat. Med 28 (11), Article 11. 10.1038/s41591-022-02001-z.

Yonker LM, Gilboa T, Ogata AF, Senussi Y, Lazarovits R, Boribong BP, Bartsch YC, Loiselle M, Rivas MN, Porritt RA, Lima R, Davis J.P. Farkas, Burns MD, Young N, Mahajan VS, Hajizadeh S, Lopez XIH, Kreuzer J, Morris R, Fasano A, 2021. Multisystem inflammatory syndrome in children is driven by zonulin-dependent loss of gut mucosal barrier. J. Clin. Invest 131 (14), e149633 10.1172/JCI149633.

Zeng N, Zhao Y-M, Yan W, Li C, Lu Q-D, Liu L, Ni S-Y, Mei H, Yuan K, Shi L, Li P, Fan T-T, Yuan J-L, Vitiello MV, Kosten T, Kondratiuk AL, Sun H-Q, Tang X-D, Liu M-Y, Lu L, 2023. A systematic review and meta-analysis of long term physical and mental sequelae of COVID-19 pandemic: Call for research priority and action. Mol. Psychiatry 28 (1), 423–433. 10.1038/s41380-022-01614-7. [PubMed: 35668159]

Zhang S, Mark KS, 2012. α1-Acid glycoprotein induced effects in rat brain microvessel endothelial cells. Microvasc. Res 84 (2), 161–168. 10.1016/j.mvr.2012.05.003. [PubMed: 22633841]

Zheng Y, Zhao J, Li J, Guo Z, Sheng J, Ye X, Jin G, Wang C, Chai W, Yan J, Liu D, Liang X, 2021. SARS-CoV-2 spike protein causes blood coagulation and thrombosis by competitive binding to heparan sulfate. Int. J. Biol. Macromol 193, 1124–1129. 10.1016/j.ijbiomac.2021.10.112. [PubMed: 34743814]

Box 1

Peripheral blood vascular health analytes

Fibrinogen is a protein commonly associated with coagulation (Pretorius et al., 2022), but is also a classic acute phase reactant in that inflammatory insults drive significantly increased liver expression and concentration in general blood circulation (Luyendyk et al., 2019). Furthermore, fibrinogen specifically induces a sustained glial response at the perivascular spaces surrounding neurovasculature, a process worsened by blood–brain barrier disruption during neuroinflammation (Davalos et al., 2012).

α2-macroglobulin is an extracellular macromolecule mainly known for its role as a broad-spectrum protease inhibitor, but also has a role facilitating immune cell migration to vasculature. For example, α2-macroglobulin aids neutrophils through stimulation of their capacity to migrate and bind to vascular endothelial cells, and to phagocytose and kill pathogens (Vandooren & Itoh, 2021).

Orosomucoid (also called alpha-1-acid glycoprotein or AGP) is known as an acute phase protein synthesized by liver, but can also be synthesized by several other tissues including brain under different physiological conditions as well as pathological conditions such as stroke and metabolic syndrome (Li et al., 2019). In a well-characterized in vitro blood–brain barrier model, human orosomucoid showed a dose-dependent effect on the permeability of microvessel endothelial cells (Zhang & Mark, 2012).

Fetuin A was previously called pp63 or countertrypin and is a multifunctional protein made by the liver and some secretory tissues. Its role in cardiovascular health is multifactorial including protective effects such as mitigation of calcification but it is also associated with worse prognosis in cardiovascular disease and diabetes. Fetuin A may act as an endogenous ligand for TLR4 receptors (Chekol Abebe et al., 2022).

sL-selectin (soluble leukocyte selectin) is also called CD62L and is a cell adhesion molecule that is expressed on most circulating leukocytes and facilitates endothelial adhesion and transendothelial migration of activated immune cells (Ivetic et al., 2019; Seekamp et al., 2001), which in turn would activate local glia. A study of acute COVID patients found that patients with severe COVID-19 had greater frequencies of CD4+ T cells expressing CD62L, in particular severe patients with hypertension (Lesteberg et al., 2023).

Pentraxin-2 (also called serum amyloid P component or SAP) is a short pentraxin protein like C-reactive protein and is a component of the humoral arm of the innate immune system, involved in infection resistance and tissue remodeling. Pentraxin-2 binds to organisms such as viruses, bacteria, and fungi (Doni et al., 2021). In mice it was also found to regulate the interaction between macrophage activation and coagulation cascades and is thought to be involved in the pathogenic buildup of amyloid fibrils by reducing normal proteolytic cleavage (Muczynski et al., 2017).

Haptoglobin protein circulating in plasma scavenges extracellular hemoglobin and is thought to have a protective effect against hemoglobin-induced vasoconstriction, however in murine models vascular endothelial dysfunction prevents this function (Graw et al.,

2017). The gut permeability marker zonulin, which is increased in the post-acute-COVID condition multisystem inflammatory syndrome in children (MIS-C) (Yonker et al., 2021) is the precursor for haptoglobin-2.

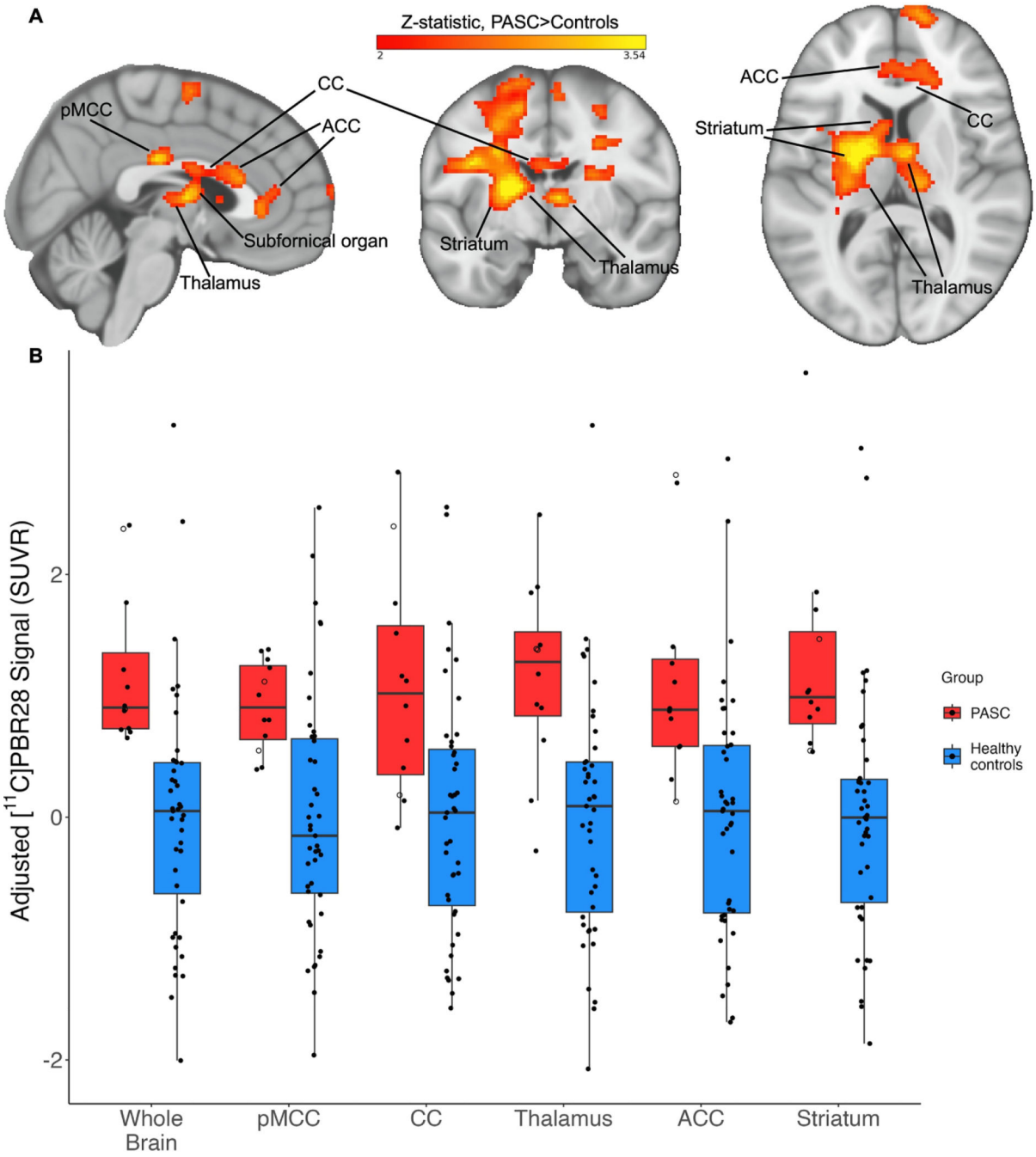

Fig. 1.

(A): Example slices through sagittal (x = 3), coronal (y = −7), and axial (z = 10) sections of the 12 PASC > 43 control group-level unpaired (between-groups) comparison, showing the pattern of increased [^{11}C]PBR28 signal (shown in neurological convention). Color bar: threshold min. *Z* score of 2 and max. 3.54. **(B)**: PET signal data extracted from individual study participants, depicted from the primary whole-brain analysis and across five example bilateral brain regions. Y-axis data points represent the mean SUVR values of significant voxels within each significant cluster region, with each structure's data normalized to the

control average. PASC participants hospitalized during their acute COVID-19 illness are indicated with an open circle. Brain regions are anatomically defined by the Harvard-Oxford Atlas (thalamus, ACC, striatum) or CC by the Jüelich Atlas at >70% probability threshold. In the case of the pMCC, we used the Harvard-Oxford posterior cingulate anatomical mask, but the activation cluster was only within pMCC. In the PASC group, the two hospitalized cases are depicted by open circles. pMCC = posterior midcingulate cortex; CC = corpus callosum; ACC = anterior cingulate cortex.

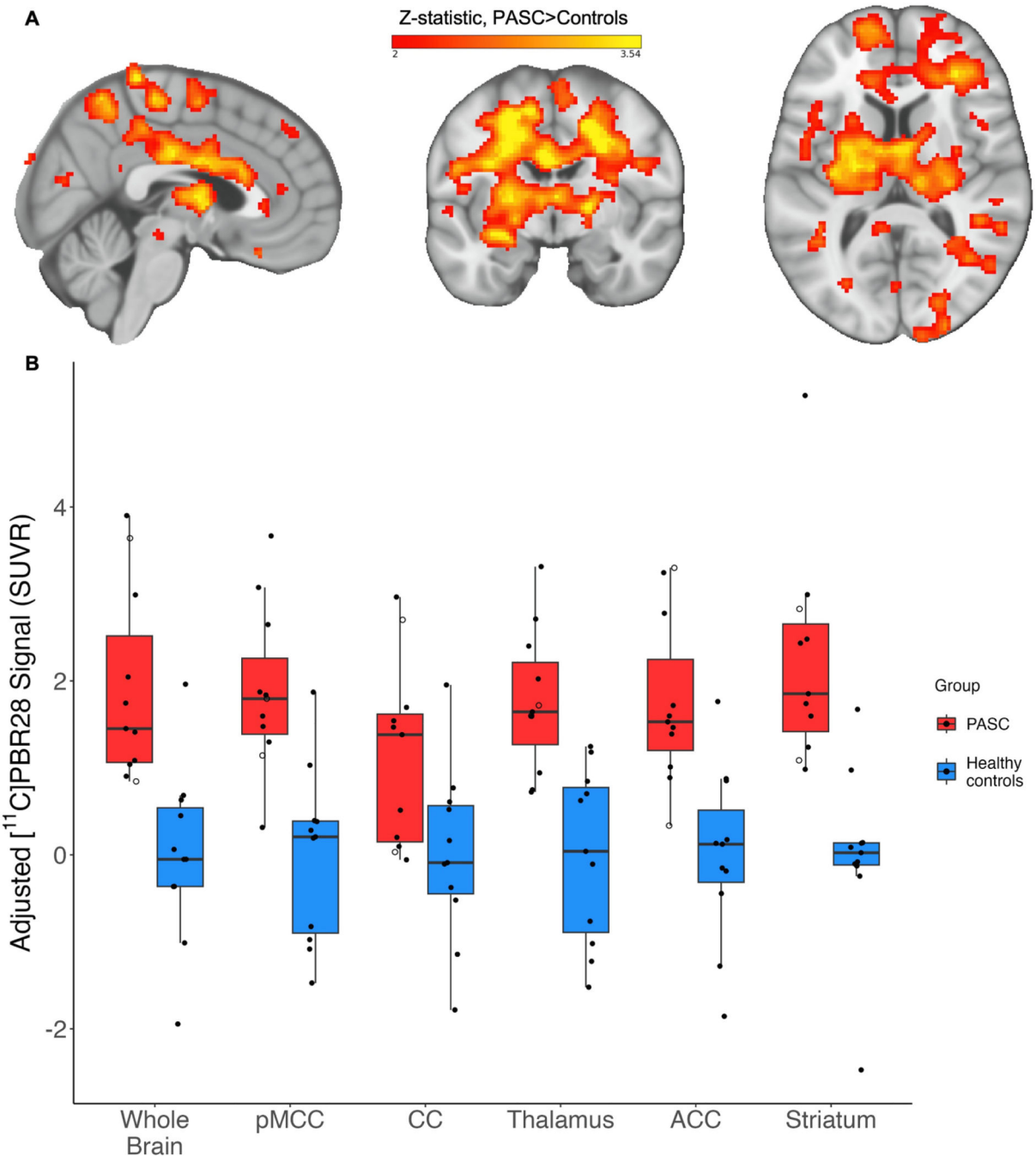

Fig. 2.

To validate our primary results, we performed a second analysis using a paired approach in which each PASC participant was matched to a control participant for genotype, sex, and age ±5 years. Because no control participant fit these criteria for one PASC participant, they were left out of the paired validation analysis. Genotype and sex were directly matched; neither age nor cerebellum SUV nor injected dose differed between cases and controls (p > .05). **(A)**: Example slices through sagittal (x = 3), coronal (y = −7), and axial (z = 10) sections of the 11 PASC > 11 control group-level unpaired validation comparison, showing

the statistically significant pattern of increased [^{11}C]PBR28 signal. **(B)**: Individual PET signal data depicted as described for Fig. 1B. Color bar: threshold min. *Z* score of 2 and max. 3.54. (Figure is shown in neurological convention).

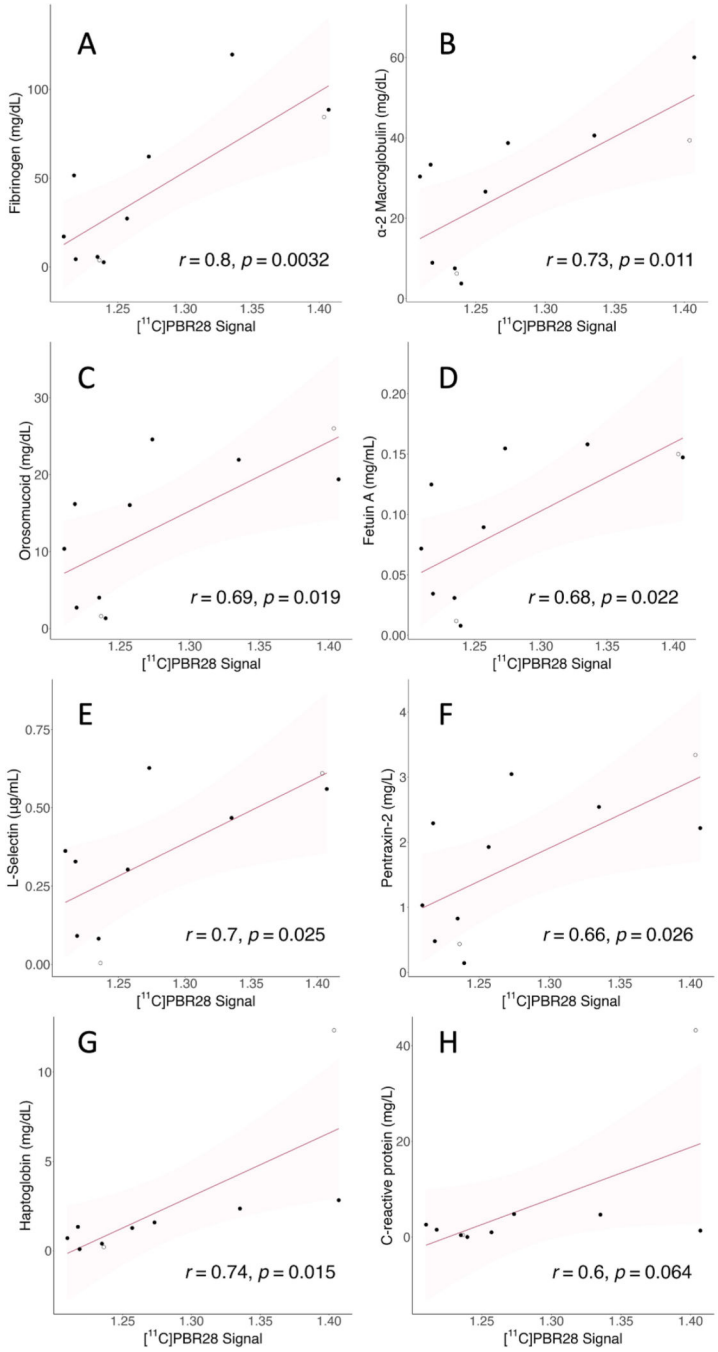

Fig. 3.

Correlations between vascular health analytes and PET signal. Y-axis shows analyte concentration; units vary. X-axis shows mean PET SUVR values extracted from the whole-brain significant cluster of each individual. Shadow represents the 95% confidence interval, all *p*-values are reported two-tailed. See Box 1 for analyte descriptions and Table 3 for Pearson's *r* values. **A**. Fibrinogen; **B**. α−2 macroglobulin; **C**. Orosomucoid; **D**. Fetuin A; **E**. sL-selectin; **F**. Pentraxin-2; **G**. Haptoglobin; **H**. C-reactive protein.

Table 1

In the primary PET comparison (i.e., n = 12 PASC vs. n = 43 control), an unpaired *t*-test or Chi-square revealed no significant difference between PASC and control groups in age, genotype frequency, BMI, or injected dose. Reflecting the sex distribution of PASC (Bai et al., 2022), there was a higher proportion of female participants in the PASC group relative to the larger historical control group. In this primary analysis, we statistically controlled for genotype and sex.

	PASC	Control	Statistics
Age [mean (SD)]	47.25 yr (14.19)	50.86 yr (14.19)	$t(53)=0.84$, $p=.20$
Sex	F=10, M=2	F=17, M=26	$X^2(1.55)=7.20$, $p=.007$
Genotype count	GG=5, GA=7	GG=27, GA=16	$X^2(1.55)=1.72$, $p=.19$
BMI	27.25 (5.01)	26.19 (4.96)	$t(53)=0.66$, $p=.51$
Injected Dose	13.64 mCi (1.90)	13.26 mCi (1.58)	$t(53)=0.70$, $p=.49$

Table 2

Peak voxel coordinates from brain regions significantly increased in PASC versus controls in whole-brain [^{11}C]PBR28 voxelwise comparison.

Region with local peak	*Z* value	MNI coordinates (x,y,z)	Cohen's *d* value
Posterior midcingulate	3.54	4, −22, 28	0.95
Corpus callosum	2.94	3, 20, 18	0.76
Thalamus (L)	3.54	−20, −2, 8	0.92
Basal ganglia (L)	3.54	−14, −6, 15	0.90
Superior frontal gyrus (R)	3.54	14, 38, 40	1.08
Subfornical organ (estimated)	3.09	4, −7, 8	0.84
Anterior midcingulate	2.95	4, 19, 19	0.72
Precentral gyrus (R)	3.54	36, 1, 36	1.12
Postcentral gyrus (R)	3.54	40, −18, 40	0.97
Retrolenticular internal capsule (L)	3.54	−28, −38, 18	0.85
Superior corona radiata (L)	3.54	−26, −6, 32	

Table 3

Vascular disease-related blood analytes that significantly correlated with whole-brain [^{11}C]PBR28 uptake values extracted from the significant cluster in the PASC group.

Peripheral blood vascular related analyte	Whole brain PET signal correlation
Fibrinogen	$r(9) = .80$, $p = .0032$
α2-macroglobulin	$r(9) = .73$, $p = .011$
Orosomucoid (alpha-1-acid glycoprotein or AGP)	$r(9) = .69$, $p = .019$
Fetuin A	$r(9) = .68$, $p = .022$
sL-selectin (soluble leukocyte selectin)	$r(8) = .70$, $p = .025$
Pentraxin-2	$r(9) = .66$, $p = .026$
Haptoglobin	$r(8) = .74$, $p = .015$